appears that the insertion of a hydrogen molecule has the effect of filtering out one of these five channels, with nearly perfect transmission.

It would be interesting to attempt to extend our technique to more complex molecules with built-in functional groups. Although most organic molecules are expected to have a conductance many orders of magnitude below the quantum unit, our experiments confirm[30] that full transmission of a single channel is possible when the coupling to the leads is sufficiently strong. Very recently, two groups have demonstrated conductance through single metal–organic molecules[31,32], for which the charge state of the metal ions could even be controlled by a gate electrode. Instead of using mechanical adjustment of the contact size as in our experiments, the size of the metal contacts to the molecule was reduced by exploiting electromigration. The tools needed to study and control electron transport at the single-molecule level are being rapidly developed. □

Received 8 May; accepted 29 August 2002; doi:10.1038/nature01103.

1. Aviram, A. & Ratner, M. (eds) *Molecular Electronics: Science and Technology* (Annals of the New York Academy of Sciences, New York, 1998).
2. Langlais, V. J. *et al.* Spatially resolved tunneling along a molecular wire. *Phys. Rev. Lett.* **83,** 2809–2812 (1999).
3. Gao, H. J. *et al.* Reversible, nanometer-scale conductance transitions in an organic complex. *Phys. Rev. Lett.* **84,** 1780–1783 (2000).
4. Collier, C. P. *et al.* Electronically configurable molecular-based logic gates. *Science* **285,** 391–394 (1999).
5. Reed, M. A., Chen, J., Rawlett, A. M., Price, D. W. & Tour, J. M. Molecular random access memory cell. *Appl. Phys. Lett.* **78,** 3735–3737 (2001).
6. Metzger, R. M. & Cava, M. P. in *Molecular Electronics: Science and Technology* (eds Aviram, A. L. & Ratner, M.) 95–115 (Annals of the New York Academy of Sciences, New York, 1998).
7. Chen, J., Reed, M. A., Rawlett, A. M. & Tour, J. M. Large on-off ratios and negative differential resistance in a molecular electronic device. *Science* **286,** 1550–1552 (1999).
8. Reed, M. A., Zhou, C., Muller, C. J., Burgin, T. P. & Tour, J. M. Conductance of a molecular junction. *Science* **278,** 252–254 (1997).
9. Kergueris, C. *et al.* Electronic transport through a metal-molecule-metal junction. *Phys. Rev. B* **59,** 12505–12513 (1999).
10. Reichert, J. *et al.* Driving current through single organic molecules. *Phys. Rev. Lett.* **88,** 176804 (2002).
11. Emberly, E. G. & Kirczenow, G. Comment on "First-principles calculation of transport properties of a molecular device". *Phys. Rev. Lett.* **87,** 269701 (2001).
12. Muller, C. J., van Ruitenbeek, J. M. & de Jongh, L. J. Experimental observation of the transition from weak link to tunneljunction. *Physica C* **191,** 485–504 (1992).
13. van Ruitenbeek, J. M. in *Mesoscopic Electron Transport* (eds Sohn, L. L., Kouwenhoven, L. P. & Schön, G.) 549–579 (Kluwer Academic, Dordrecht, 1997).
14. Rubio, G., Agraït, N. & Vieira, S. Atomic-sized metallic contacts: mechanical properties and electronic transport. *Phys. Rev. Lett.* **76,** 2302–2305 (1996).
15. Agraït, N., Levy Yeyati, A. & van Ruitenbeek, J. M. Quantum properties of atomic-sized conductors. Preprint cond-mat/0208239 at ⟨http://xxx.lanl.gov⟩ (2002).
16. Yanson, I. K. Nonlinear effects in the electric conductivity of point junctions and electron-phonon interaction in metals. *Zh. Eksp. Teor. Fiz.* **66,** 1035–1050 (1974); *Sov. Phys. JETP* **39,** 506–513 (1974).
17. Jansen, A. G. M., van Gelder, A. P. & Wyder, P. Point-contact spectroscopy in metals. *J. Phys. C* **13,** 6073–6118 (1980).
18. Untiedt, C., Rubio Bollinger, G., Vieira, S. & Agraït, N. Quantum interference in atomic-sized point-contacts. *Phys. Rev. B* **62,** 9962–9965 (2000).
19. Agraït, N., Untiedt, C., Rubio-Bollinger, G. & Vieira, S. Onset of dissipation in ballistic atomic wires. *Phys Rev. Lett.* **88,** 216803 (2002).
20. Bonča, J. & Trugman, S. A. Effect of inelastic processes on tunneling. *Phys. Rev. Lett.* **75,** 2566–2569 (1995).
21. Emberly, E. G. & Kirczenow, G. Landauer theory, inelastic scattering and electron transport in molecular wires. *Phys. Rev. B* **61,** 5740–5750 (1999).
22. Stipe, B. C., Rezaei, M. A. & Ho, W. Single-molecule vibrational spectroscopy and microscopy. *Science* **280,** 1732–1735 (1998).
23. van den Brom, H. E. & van Ruitenbeek, J. M. Quantum suppression of shot noise in atomic-size metallic contacts. *Phys. Rev. Lett.* **82,** 1526–1529 (1999).
24. Khotkevich, A. V. & Yanson, I. K. *Atlas of Point Contact Spectra of Electron-phonon Interactions in Metals* (Kluwer Academic, Dordrecht, 1995).
25. Ludoph, B. & van Ruitenbeek, J. M. Conductance fluctuations as a tool for investigating the quantum modes in atomic-size metallic contacts. *Phys. Rev. B* **61,** 2273–2285 (2000).
26. Frisch, M. *et al.* J. Gaussian 98, Revision A.5 (Gaussian, Inc., Pittsburgh, Pennsylvania, 1998).
27. Andrae, D., Häußermann, U., Dolg, M., Stoll, H. & Preuss, H. Energy-adjusted ab initio pseudopotentials for the 2nd and 3rd row transition-elements. *Theor. Chim. Acta* **77,** 123–141 (1990).
28. Becke, A. D. Density-functional thermochemistry. III. The role of exact exchange. *J. Chem. Phys.* **98,** 5648–5652 (1993).
29. Lang, N. D. Resistance of atomic wires. *Phys. Rev. B* **52,** 5335–5342 (1995).
30. Lang, N. D. & Avouris, Ph. Electrical conductance of individual molecules. *Phys. Rev. B* **64,** 125323 (2001).
31. Park, J. *et al.* Coulomb blockade and the Kondo effect in single-atom transistors. *Nature* **417,** 722–725 (2002).
32. Liang, W., Shores, M. P., Bockrath, M., Long, J. R. & Park, H. Kondo resonance in a single-molecule transistor. *Nature* **417,** 725–729 (2002).

Acknowledgements We acknowledge discussions with A. Levy Yeyati and S. K. Nielsen, and we thank D. Bakker and M. Pohlkamp for assistance in the experiments. C.U. and Y.N. were supported by European Community Marie Curie fellowships.

Competing interests statement The authors declare that they have no competing financial interests.

Correspondence and requests for materials should be addressed to J.M.v.R. (e-mail: ruitenbe@phys.leidenuniv.nl).

Relationship between local structure and phase transitions of a disordered solid solution

Ilya Grinberg, Valentino R. Cooper & Andrew M. Rappe

Department of Chemistry and Laboratory for Research on the Structure of Matter, University of Pennsylvania, Philadelphia, Pennsylvania 19104-6323, USA

The $Pb(Zr,Ti)O_3$ (PZT) disordered solid solution is widely used in piezoelectric applications owing to its excellent electromechanical properties. Six different structural phases have been observed for PZT at ambient pressure, each with different lattice parameters and average electric polarization. It is of significant interest to understand the microscopic origin of the complicated phase diagram and local structure of PZT[1–8]. Here, using density functional theory calculations, we show that the distortions of the material away from the parent perovskite structure can be predicted from the local arrangement of the Zr and Ti cations. We use the chemical rules obtained from density functional theory to create a phenomenological model to simulate PZT structures. We demonstrate how changes in the Zr/Ti composition give rise to phase transitions in PZT through changes in the populations of various local Pb atom environments.

PZT is a perovskite ABO_3 alloy with random B-site occupation by either Zr or Ti at all phases and compositions. The six structural phases that have been observed at ambient pressure are an antiferroelectric phase for compositions near $PbZrO_3$, ferroelectric low-temperature and high-temperature rhombohedral (R) phases for most Zr-rich alloys, a newly discovered monoclinic[2] (M) ferroelectric phase near 50% Zr/50% Ti ('50/50') composition, a tetragonal (T) ferroelectric phase for Ti-rich alloys, and a cubic paraelectric phase for all compositions at sufficiently high temperature. All phases of the material are generated by distortions from the same high-symmetry cubic parent structure, and are distinguished only by differing lattice parameters and by the directions of the structural distortions which give rise to the average polarization **P** of the material.

We have studied the local structure of PZT using *ab initio* density functional theory (DFT) calculations with the local density approximation (LDA) exchange-correlation functional. To obtain the ground-state structure, we minimize the energy with respect to ionic coordinates, starting with randomized perfect perovskite positions with no symmetry imposed. To represent the bulk nature of the material we use periodic boundary conditions. However, the disorder in the B-cation arrangement makes small, DFT-accessible supercells an inexact representation of the real material. This can be seen from the narrow peaks in the neutron scattering pair-distribution function (PDF) (representing the ensemble average distribution of interatomic distances in the crystal) of the DFT-obtained structure (Fig. 1). Increasing the size of the supercell

quickly becomes computationally intractable, and we therefore take a different approach.

To examine the range of distortion behaviour and to correlate structural motifs with the local environment, we carry out calculations on all possible B-cation arrangements of $4\times2\times1$ 40-atom supercells at 50/50 composition (Fig. 2) as well as several 60-atom supercells and 30-atom supercells at Ti-rich and Zr-rich compositions. These supercells can be thought of as snapshots of small regions of the real disordered material. As a result, our DFT study identifies distortion patterns and correlations which will also be present in the real disordered material. Predictable dependence of motifs on local structure allows construction of a model that encapsulates the behaviour of the material. Such a model can then be used to study large supercells inaccessible with DFT.

The most energetically important oxygen distortion motif is the contraction (expansion) of Ti–O (Zr–O) bonds by 0.1–0.2 Å in the direction of the neighbouring Zr(Ti) atoms. The BO_6 octahedra have well-defined volumes: 69–71 $Å^3$ for ZrO_6 and 63–65 $Å^3$ for TiO_6. The oxygen complexes also rotate by 0–5° (ref. 7).

To relate the cation behaviour to local structure, we examine the distortions of the cations from the centres of their oxygen cages. In the perovskite structure, each oxygen participates in four PbO_{12} cages and two B-cation O_6 cages. We define the position of a cage centre as the weighted average of the positions of all the oxygen atoms that participate in the cage, such that the cage centre has an effective charge of the same magnitude as its cation. In an ideal perovskite, the centre of the cage and the metal ion are located at the same point, and polarization is therefore zero. In the actual, lower-symmetry structure such as that shown in Fig. 2, the distortions of the metal ions away from the centre of the oxygen cages generate local polarization and give rise to ferroelectricity.

Our calculations show that Ti and Zr move 0.1–0.3 Å off-centre, with Ti distortions larger and directed more toward one O atom than those of Zr. Pb ions move off-centre by 0.4–0.5 Å, creating four short Pb–O bonds, in agreement with experimental results[9]. Confirming previous interpretation of PZT PDFs[8], we find that (100), (211) or (110) Pb distortions are preferred over (111), even in the rhombohedral phase where overall **P** is along (111). Unlike the B-cation distortions, the Pb distortion directions are sensitive to the B-cation environment. Pb distortions are toward Ti neighbours and away from Zr neighbours. This is indicated by the difference in the A–B cation distances; the Pb–Ti distances range from 3.27 to 3.4 Å, while Pb–Zr distances range from 3.35 to 3.6 Å. The Pb distortions also conform to the overall polarization as much as possible. The agreement with overall polarization and the Pb atom preference to avoid Zr can either cooperate or compete, as can be seen from Fig. 2. In the case of Pb atoms 1 and 2 in Fig. 2, both driving forces cooperate. However, in the case of Pb atoms 3 and 4, the local preference to move toward Ti conflicts with the desire to align with overall polarization. This competition results in a compromise, with distortions predominantly along (100) for these Pb atoms. We also find that the alignment of Pb distortions with the average polarization depends on the composition. The scatter of the Pb distortions from the overall polarization vector is 25° for the Zr-rich R phase, 15° for the 50/50 M phase and 10° for the Ti-rich T phase.

Pb distortion directions are sensitive to local structure, whereas the B-cation distortion directions are not. This difference can be understood by considering the differences in the local environment of the A and B cations in the ideal perovskite structure. For Pb atoms, the oxygen nearest-neighbour shell has 12-fold symmetry, but symmetry is broken in the B-cation next-nearest-neighbour shell. Zr is a larger ion than Ti, which means that the purely repulsive interaction between Pb and B cations will be stronger for Pb–Zr than for Pb–Ti. On the other hand, all B-cation environments have six-fold symmetry in the oxygen cage and eight-fold symmetry in the Pb next-nearest-neighbour shell. Therefore, B-cation distortions do not display a strong dependence on local structure and align closely with the Pb atom distortions. In agreement with the suggestion of ref. 8, we therefore identify the Pb distortions as the determining factor for the average structure of the material.

We now examine how the interplay of the dipole interactions and local A–B cation repulsion gives rise to disparate structural phases at different Zr/Ti compositions. The Pb distortions are produced by a hierarchy of interactions. In all PZT phases, Pb tends to move toward (100), (010) and (001) faces in order to form stronger bonds with four of its oxygen neighbours, without closely encountering B cations. (A move by Pb along (111) would be directly toward a B cation, which would incur a high energy cost.) Each Pb has a choice of six such faces. The Pb atoms tend to move toward the face that is closest to the overall polarization direction **P** in order to lower the dipole interaction energy. If this face is Ti-rich (0 or 1 Zr), the Pb will move toward it strongly (perhaps with a small tilt away from the Zr or toward **P**). A neutral face (2 Zr and 2 Ti) permits moderate Pb motion toward it, with a significant tilt. Zr-rich (3 or 4 Zr) faces cause the Pb to tend to move toward a different face to avoid large Pb–Zr repulsion. The relative amounts of Zr-rich, neutral and Ti-rich faces are strongly dependent on Zr/Ti composition (Fig. 3).

In the Ti-rich region of the phase diagram, Ti-rich faces dominate and a T phase (with Pb distortions aligning in one direction) minimizes the dipole alignment energy without raising the repulsion energy. The R phase, with Pb distortions in a variety of directions, minimizes the local repulsion energy just as well as the T phase, but results in a larger dipole interaction energy cost. Therefore the T phase is preferred.

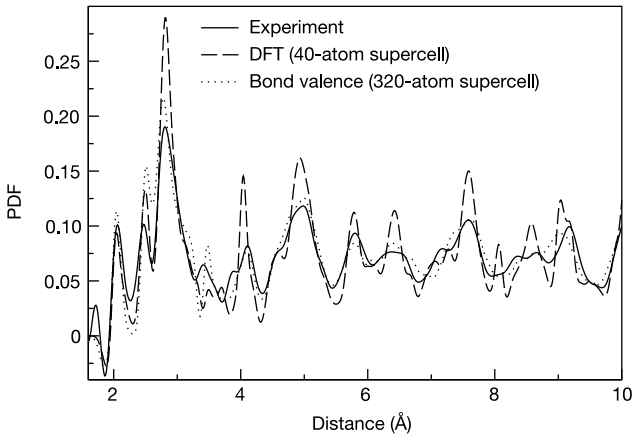

Figure 1 Pair distribution functions (PDFs) for PZT with 50% Zr/50% Ti. Data are from experiment[8], DFT, and the bond-valence model. Similar agreement with experiment is obtained with the bond-valence model at 40/60 and 60/40 compositions.

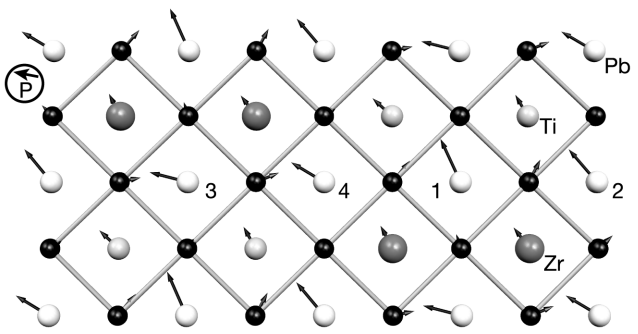

Figure 2 Projection of the $4\times2\times1$ 50/50 supercell DFT PZT structure on the *x*–*y* plane. The oxygen octahedra are depicted by diamonds, and distortions from the ideal cubic perovskite positions are shown by arrows. Pb atoms are 1/2 unit cell above the plane, and apical O atoms are omitted.

In the Zr-rich region of the phase diagram, Zr-rich faces dominate and T Pb distortions with small angle scatter can minimize the dipole interaction energy only by suffering a high A–B repulsion energy cost. Therefore the R phase is preferred. Here, the Pb atoms distort in a variety of directions toward the available Ti-rich faces to reduce local repulsion cost. However, this large variation in distortion direction raises the dipole interaction energy. Unlike the Ti-rich T phase, the Zr-rich R phase is a disordered compromise structure[8] where trade-offs are made between the two components of the energy. This explains the difference in angle scatter at various compositions of PZT found by DFT calculations.

At around 50/50 composition, equal amounts of Zr-rich, Ti-rich and neutral faces are present in the material. A concerted distortion in a tetragonal direction can be accommodated by the Pb atoms encountering a Ti-rich or a neutral face. However, the Pb atoms encountering a Zr-rich face must distort in other directions to minimize the A–B repulsion, creating a (211) polarization of the monoclinic phase.

We have created a model to quantify our insights, and to demonstrate that B-cation disorder combined with simple interatomic interactions is sufficient to reproduce and explain the complicated behaviour of PZT as seen by disordered PDFs and compositional phase transitions. The model contains physically intuitive interactions, and can be applied to any perovskite material. We use Ewald summation to compute the long-range Coulomb interaction energy E_{ew}. To simulate bonding we use Brown's rules of valence[10,11], which have been tested in many different types of oxides. In the bond valence theory, the bond order of each cation–oxygen bond can be expressed as a power law in the bond distance R_{ij}. Each atom has a desired valence (or total bond order) V_i^0 (+2 for Pb, +4 for Zr and Ti, and −2 for O), so the bond valence energy is

$$E_{bv} = A_{bv} \sum_i \left[V_i^0 - \sum_j (R_{ij}/R_{ij}^0)^{-N_{ij}} \right]^{\alpha_i} \qquad (1)$$

The j sum runs over all nearest neighbours of the ith atom, R_{ij}^0 and N_{ij} relate bond strength to distance, and A_{bv} and α_i control how stringently the desired bond valences are achieved. As a simple illustration, the ideal perovskite structure would yield valences of 1.5 for Pb, 4.5 for Zr, and 3.6 for Ti. To increase their valences, Pb and Ti must move off-centre and form shorter, stronger bonds. To decrease its valence, Zr must increase its octahedral cage volume.

For better agreement with DFT results, the total energy also includes short-range repulsions and sum rules on short bonds:

$$E = E_{ew} + E_{bv} + \sum_{ij} A_{ij} e^{k_{ij}(R_{ij} - D_{ij})} + Q \sum_i (S_i - S_i^0)^\beta \qquad (2)$$

A_{ij}, D_{ij}, and k_{ij} control the repulsion strength, to keep the atoms from making unphysically short distances. S_i is the sum of the three shortest Ti–O distances, S_i^0 is the desired value of this sum, and Q and β govern the strength of sum rule.

We parameterize our model to reproduce bond lengths, cage volumes and angle scatter found in DFT calculations, and to give peaks of correct width in the PDF. We then apply the model to study a series of larger 4×4×4 320-atom supercells with various random B-cation arrangements and compositions, minimizing the energy with respect to ionic coordinates in the same fashion as in DFT calculations. After minimization we find that the average valence is 4.02 ± 0.05 for Zr and Ti, 2.0 ± 0.08 for O, and 1.98 ± 0.05 for Pb. Our model correctly predicts the compositional phase transitions from rhombohedral at 60/40, to monoclinic at 50/50 to tetragonal at 40/60. This model also yields computed PDFs in excellent agreement with the experimental PDFs (Fig. 1). Thus the interactions we found through DFT calculations, when combined with large disordered cells, result in the rich structure found experimentally in PZT.

As the same physical principles (Ewald summation, Brown's bond-valence interactions, short-range repulsions) govern a wide class of solids, we expect this model to have wide applicability to the study of disordered systems. Expressing the energy of the system in terms of intuitive interatomic interactions allows us to link atomic properties with the statistical distribution of local structural motifs and with macroscopic properties. This multiscale modelling approach may close the gap between the goal of the material's design (favourable macroscopic properties) and the techniques used to achieve these goals (typically the variations in the atomic composition of the material). We have shown that a simple statistical interplay of well-known chemical interactions obtained through first-principles calculations, coupled with disorder, can give rise to rich local structure and to complex phase behaviour in a solid solution. □

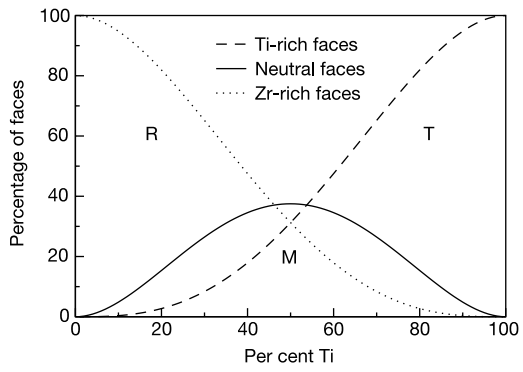

Figure 3 Populations of Ti-rich, Zr-rich and neutral faces in disordered PZT as a function of Ti content. R, M and T label the rhombohedral, monoclinic and tetragonal regions of the phase diagram.

Methods

In the bond-valence model calculations we use use formal charges (+2 for Pb, +4 for Zr and Ti, and −2 for O) for electrostatic interactions. The bond-valence parameters are $A_{bv} = 80.0$, $R_{Pb-O} = 2.021$, $R_{Zr-O} = 1.933$, $R_{Ti-O} = 1.841$, $N_{Pb-O} = 5.51$, $N_{Zr-O} = 6.0$, $N_{Ti-O} = 5.211$, $\alpha_{Pb} = 1.25$, $\alpha_{Zr} = 2.0$, $\alpha_{Ti} = 2.0$, $\alpha_O = 1.5$, $S_{Ti}^0 = 5.76$, $\beta = 1.4$, $Q = 20$, $A_{Pb-O} = 50.0$, $A_{Zr-O} = 50.0$, $A_{Ti-O} = 50.0$, $A_{Pb-Zr} = 175.0$, $A_{Pb-Ti} = 175.0$, $k_{Pb-O} = 25.0$, $k_{Zr-O} = 20.0$, $k_{Ti-O} = 20.0$, $k_{Pb-Zr} = 60.0$, $k_{Pb-Ti} = 60.0$, $D_{Pb-O} = 2.27$, $D_{Zr-O} = 1.80$, $D_{Ti-O} = 1.45$, $D_{Pb-Zr} = 3.34$, $D_{Pb-Ti} = 3.23$. A_{bv} and Q are in eV. R_{ij} and D_{ij} are in Å.

Received 24 April; accepted 10 September 2002; doi:10.1038/nature01115.

1. Bellaiche, L., Garcia, A. & Vanderbilt, D. Finite-temperature properties of $Pb(Zr_{1-x}Ti_x)O_3$ alloys from first principles. *Phys. Rev. Lett.* **84,** 5427–5430 (2000).
2. Noheda, B. *et al.* A monoclinic ferroelectric phase in the $Pb(Zr_{1-x}Ti_x)O_3$ solid solution. *Appl. Phys. Lett.* **74,** 2059–2061 (1999).
3. Cohen, R. E. Origin of ferroelectricity in perovskite oxides. *Nature* **358,** 136–138 (1992).
4. Fu, H. & Cohen, R. E. Polarization rotation mechanism for ultrahigh electromechanical response in single-crystal piezoelectrics. *Nature* **403,** 281–283 (2000).
5. Ghosez, P., Cockayne, E., Waghmare, U. V. & Rabe, K. M. Lattice dynamics of $BaTiO_3$, $PbTiO_3$, and $PbZrO_3$: A comparative first-principles study. *Phys. Rev. B* **60,** 836–843 (1999).
6. Saghi-Szabo, G., Cohen, R. E. & Krakauer, H. First-principles study of piezoelectricity in tetragonal $PbTiO_3$ and $PbZr_{1/2}Ti_{1/2}O_3$. *Phys. Rev. B* **59,** 12771–12776 (1999).
7. Fornari, M. & Singh, D. J. Possible coexistence of rotational and ferroelectric lattice distortions in rhombohedral $PbZr_xTi_{1-x}O_3$. *Phys. Rev. B* **63,** 092101 (2001).
8. Dmowski, W., Egami, T., Farber, L. & Davies, P. K. in *Fundamental Physics of Ferroelectrics—Eleventh Williamsburg Ferroelectrics Workshop* (ed. Cohen, R. E.) 33–44 (AIP, Woodbury, New York, 2001).
9. Egami, T., Dmowski, W., Akbas, M. & Davies, P. K. in *First-Principles Calculations for Ferroelectrics—Fifth Williamsburg Workshop* (ed. Cohen, R. E.) 1–10 (AIP, Woodbury, New York, 1998).
10. Brese, N. E. & O'Keeffe, M. Bond-valence parameters for solids. *Acta. Crystallogr. B* **47,** 192–197 (1991).
11. Brown, I. D. in *Structure and Bonding in Crystals II* (eds O'Keeffe, M. & Navrotsky, E.) 1–30 (Academic, New York, 1981).

Acknowledgements We thank T. Egami, W. Dmowski and P. K. Davies for discussions and for sharing PDF data. This work was supported by the Office of Naval Research and the National Science Foundation. Computational support was provided by the High-Performance Computing Modernization Office of the Department of Defense and the Center for Piezoelectric Design. A.M.R. thanks the Camille and Henry Dreyfus Foundation for support.

Competing interests statement The authors declare that they have no competing financial interests.

Correspondence and requests for materials should be addressed to A.M.R. (e-mail: rappe@sas.upenn.edu).